16th World Congress in Computational Mechanics (WCCM)
21-26 July 2024, Vancouver, Canada
A. Korobenko, M. Laforest, S. Prudhomme, R. Vaziri (Eds)

MATHEMATICAL AND EXPERIMENTAL MODELING OF A STOCKBRIDGE DAMPER USED TO SUPPRESS AEOLIAN VIBRATION OF TRANSMISSION LINE CONDUCTORS

ZAKHELE M. ZONDI[1], TIYAMIKE NGONDA[2], AND MODIFY A.E. KAUNDA[3] ROB STEPHEN[4],

[1]Mangosuthu University of Technology, Department of Mechanical Engineering
511 Griffiths Mxenge Hwy, Umlazi, Durban, 4031
zakhele@mut.ac.za

[2]Cape Peninsula University of Technology
Department of Mechanical Engineering, Bellville Campus,
Bellville South Industrial, Cape Town, 7530
ngondat@cput.ac.za

[3]Cape Peninsula University of Technology
Department of Mechanical Engineering, Bellville Campus,
Bellville South Industrial, Cape Town, 7530
kaundam@live.com

[4]University of KwaZulu Natal Westville, Department of Electrical Engineering
University Rd, Westville, 3629
rob.stephen@cigre.org

Keywords: Wind-induced vibrations, Stockbridge damper, resonance frequencies.

Abstract. The asymmetric Stockbridge vibration damper is commonly employed in overhead power cables to mitigate Aeolian vibration, which is the oscillation of conductor cables within the 3–150 Hz frequency range. The damper's effectiveness is determined by its resonant frequencies, which increase power dissipation to exceed the wind-induced power input. While the basic symmetric Stockbridge damper has two resonant frequencies, the asymmetric version can exhibit up to four. Previous studies have shown that changes in the counterweight's geometry can increase the natural frequencies. This paper presents experiments on a modified asymmetric damper and uses an analytical model from Vaja et al. (2018), to confirm their findings. employed in overhead transmission lines to mitigate Aeolian vibration

1 INTRODUCTION

Generating electrical power necessitates the utilization of overhead power cables to transport it from power stations to dispersed substations situated at varying distances. However, these transmission lines are subjected to diverse wind patterns, inducing vibrations that significantly impact their longevity. Three primary wind-induced vibrations affect these transmission lines: conductor galloping, Aeolian vibration, and wake-induced oscillation [1,

2]. Wake-induced oscillation mainly affects power lines with bundled conductors, resulting from aerodynamic forces acting on the downstream conductor within the bundle as it moves in and out of the wake of the upstream conductor [3]. Strategies to mitigate this phenomenon include maintaining appropriate conductor spacing, varying sub-span lengths, and tilting the conductor bundle. Typically, this motion exhibits amplitudes within the range of 10 conductor diameters, with oscillation frequencies falling between 1 and 10 Hz [1, 2]. Conductor galloping, on the contrary, is characterized by high amplitude, low-frequency vertical conductor motion, occurring when freezing rain forms icicles and irregular ice shapes on transmission towers and conductors. High winds and uplift forces drive these icicles and conductors, inducing a galloping motion. Aeolian vibration, the most prevalent wind-induced motion, leads to fatigue and eventual overhead transmission line failure [4]. It is characterized by high frequency, ranging from 3 to 150 Hz, and low amplitude, dependent on the cable diameter [1, 5]. In this scenario, wind speeds typically fall within the range of 1 to 7 m/s, with the frequency of aeolian vibration fluctuating between 3 and 150 Hz. These variations depend on factors such as conductor diameter and wind speed, as indicated by studies conducted by [6], [7], [8], and [9].

To reduce vibration amplitudes and maintain them within permissible fatigue thresholds in transmission lines, protective mechanisms have been created and implemented. Among these, the Stockbridge-type vibration damper stands out as a widely adopted solution, initially conceived by Stockbridge in 1924. The Stockbridge damper is a turned mass absorber, only effective at certain resonance frequencies. At general frequencies, it is not a mass absorber or damper. Notably, this damper is respected for its efficiency across a diverse spectrum of frequencies, as highlighted by the findings of researchers such as [7], [10], [11], and [12].

Despite the development of a linear analytical model to reveal the characteristics of the vibration damper, a more intricate model was deemed necessary to explore the impact of nonlinear factors on its vibration characteristics [13]. Luo et al. (2016) presented a comprehensive finite element model of the Stockbridge vibration damper, wherein contact conditions were considered by employing the linear perturbation method. The investigation focused on the relationships between contact conditions and mode frequencies. The findings demonstrated the significant influence of contact conditions between each pair of damper parts on the overall structure's stiffness. The numerical model's results were in good agreement with those derived from experimental data. Lastly, the numerical model was employed to examine how the bonding material between the counterweight and steel strand cable affected the mode frequencies of the vibration damper [13].

A single distributed Jenkin element was employed to represent the damper cable of a Stockbridge damper in a simulation by Sauter and Hagedorn (2002). The objective was to replicate damper impedances based on data acquired from a previous experiment involving a segment of damper cable. The significance of such simulation models lies in their contribution to the design of new dampers, which, historically, have often been developed through a trial-and-error approach. Particularly, the exploration of the new generation of asymmetric dampers with four resonances could also be facilitated through this modeling approach. The simulation model was anticipated to yield favorable outcomes, encompassing the damper impedance's dependence on the clamp velocity amplitude. While the results obtained thus far have shown promise, there is room for improvement in the vicinity of the second resonance. Currently, an investigation is underway to determine whether the inclusion

of shear deformation and, potentially, a second Jenkin element is sufficient for achieving an accurate model [14].

Notably, the most recent model was formulated by Barry et al. (2015), Vaja et al. (2017), Vaja et al. (2018), and Yin et al., 2021. The nonlinear dynamics of a Stockbridge damper were investigated [15]. The nonlinearity in this context resulted from both damping effects and the geometric stretching of the messenger. The Stockbridge damper was conceptualized as two cantilevered beams with attached tip masses. The equations of motion and boundary conditions were derived using Hamilton's principle by Barry et al. (2015). Importantly, the developed model was valid for both symmetric and asymmetric configurations of Stockbridge dampers. The research provided explicit expressions for key parameters, including the frequency equation, mode shapes, nonlinear frequency, and modulation equations. Additionally, experiments were conducted to validate the proposed model, assessing its accuracy and reliability.

Vaja et al. (2017) conducted modeling and vibration analysis of Stockbridge dampers, highlighting the close relationship between the design of a Stockbridge damper, particularly the messenger cable, and the size of the overhead power cable. However, it was not easy to analytically model the complex geometry of the messenger. Since the messenger consisted of a bunch of thin helical wires with nonlinear contact conditions, determining an equivalent stiffness was necessary to incorporate into the analytical model [16]. The research examined the bending stiffness of the cable and discussed the effect of this stiffness on the natural frequencies. The derived equivalent stiffness accounted for the assumption of representing the messenger as a rod.

Vaja et al. (2018) addressed the necessity of enhancing the conventional Asymmetric Stockbridge damper in a recent discussion. Building upon previous investigations that highlighted the potential for maximizing resonant frequencies through changes in counterweight design, a novel vibration damper was developed. A mathematical representation of the vibration damper was presented in the research, and the results obtained from the analytical model underwent validation through a numerical model. The resonant frequencies of the Asymmetric damper were assessed using both numerical modeling techniques and experimental data [17]. The findings demonstrated a notable increase in resonant frequencies with the implementation of the new design, indicating enhanced damping performance compared to the traditional Stockbridge damper.. The study also identified the unique geometric characteristics of the novel vibration damper as adjustable parameters, suggesting potential for further optimization to enhance damping and resonance characteristics.

In their 2021 study, Yin et al. (2021) developed approximate calculation formulas for determining the natural frequencies of the one-side subsystem in a Stockbridge-type vibration damper. The researchers also performed a design sensitivity analysis on these natural frequencies, employing partial differential equations that considered multiple parameters. These parameters encompassed the length of the steel strand, the mass of the counterweight, the eccentric distance, and the radius of gyration of the counterweight. The objective of this investigation was to assess the influence of each parameter on the natural frequencies by examining the associated partial differential equations [18].

The experiment was conducted on the modified asymmetric Stockbridge damper to check if it could produce more than four resonance frequencies [19]. This paper focused on

experimental results and the analytical model was developed. The analytical model results were validated using experimental results. The messenger cable was represented as an Euler-Bernoulli beam, with an assumption of linear behavior. The equations describing motion and the conditions at boundaries were deduced utilizing Hamilton's principle [17].

2 EXPERIMENTAL SETUP

The experimental setup presents three methods that will be used in the experiments. The first experiment will be conducted on the asymmetric and modified asymmetric dampers to get the graphs of acceleration vs resonance frequency using the Puma system. The second is the VIP (Vibration Isolation Platform) Damper tests to be conducted to get graphs of force vs resonance frequency, impedance vs resonance frequency, and power vs resonance frequency. The third method will be to use the analytical model developed by Vaja et al. (2018).

2.1 Experimental setup using the Puma system

The oscillations experienced by the messenger cable of the damper involve both linear and rotational motions. Replicating these real-world vibrations in a lab necessitates costly trials of the Stockbridge damper on a testing rig. Moreover, the rotational effect on the damper is negligible, allowing it to be disregarded during experimentation. All data gathered from testing the damper using the electrodynamic shaker was derived solely from applying vertical motion to the clamp [1, 2]

The apparatus utilized for these tests is shown in Figure 1, and research studies were performed on asymmetric Stockbridge dampers sticking to the specifications outlined in the Institute of Electrical and Electronics Engineers (IEEE) 664 guidelines. A normal and modified asymmetrical Stockbridge damper has undergone testing on a shaker, with the test being repeated twice. Three accelerometers (100 mv/g) were affixed to each damper's weights, and one was attached to the shaker base using glue, as shown in Figures 2 and 3. Figure 4 shows the damper with added masses on both weights alternatively. An electro-dynamic shaker (TIRA Model, Type TV 56263/LS-340) was employed to administer an input force to the damper. An amplification apparatus was utilized to regulate the voltage or current supplied to the shaker. A computer-controlled data acquisition system served as the control mechanism, and a compressor was employed to prevent excessive loads.

Table 1 shows the masses added to the inner parts from damper number 1 to damper number 6. Each damper was tested twice to get a graph of acceleration versus frequency. In total twelve tests were conducted. The frequency range during the tests spanned from 5 to 200 Hz, with the shaker consistently operating at a fixed speed of 0.1 m/s for 30 minutes in each test.

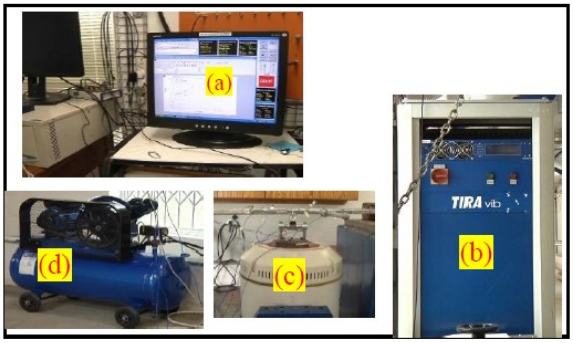

Figure 1: Components of the vibration test system on the shaker base: (a) controller. (b) Amplifier. (c) Shaker, asymmetric damper, and accelerometers (100 mv/g). (d) Compressor.

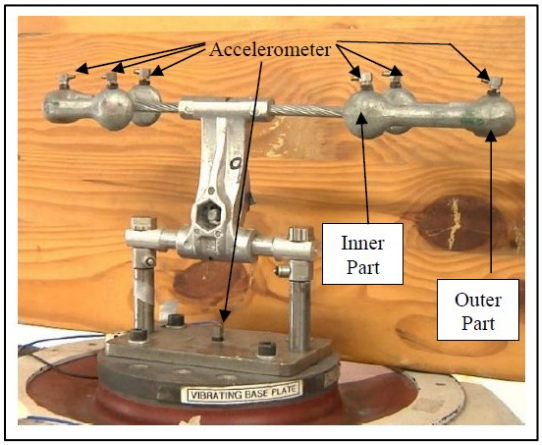

Figure 2: The damper with three accelerometers (100 mv/g) on each mass

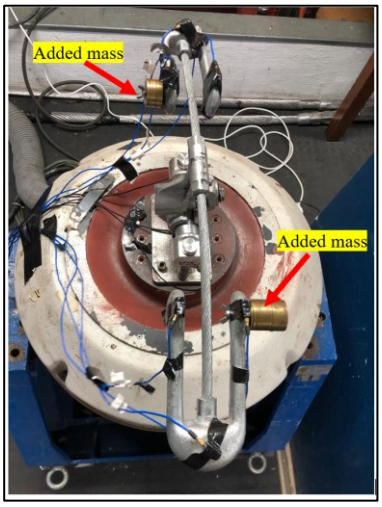

Figure 3: The damper with the addition of small masses on each side inner part of each mass

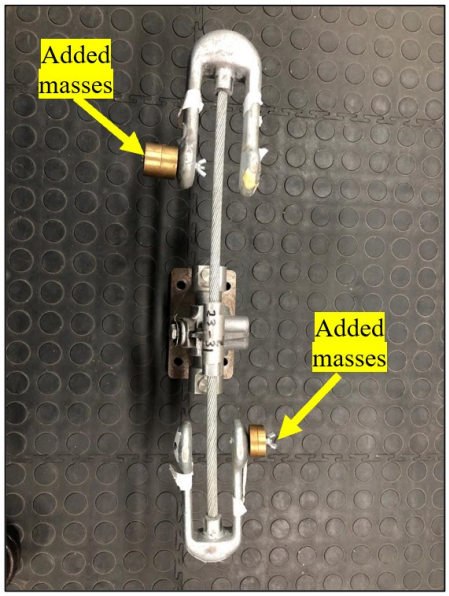

Figure 4: The top view of the damper with added masses on the inner parts of each weight.

Table 1: Sizes of added masses to the inner and the outer sides of both weights

Damper number	Masses on the smaller weight in grams	Masses on the bigger weight in grams
1	0	0
2	10	20
3	25	50
4	50	100
5	100	200
6	120	230

2.2 Experimental setup using VIP (Vibration Isolation Platform)

A second VIP (Vibration Isolation Platform) Damper tests were conducted in which each of the five dampers with different added masses and one damper with no added masses were tested separately on the shaker. VIP Damper Tests focuses exclusively on testing vibration dampers that are directly mounted on a shaker. The facility is equipped to conduct a comprehensive range of dynamic tests mandated by major international standards and specifications such as IEC, IEEE, DIN, BS, and others. Figure 5 illustrates the layout of the test stand used for evaluating the dynamic response of dampers at the VIP Damper Test

facility. The sweep test ranges between 5 and 100 Hz and the peak-to-peak (constant amplitude) was set to 0.5 mm. One accelerometer (90,74 mv/g) was stuck on the base of the shaker and two force transducers (21,43 mv/N and 21,3 mv/N) were stuck on either side of the jig as shown in Figure 6. The arrangement of added masses from damper number 1 to damper number 6 is shown in Table 1. Each damper was tested twice to get a graph of force versus frequency, power versus frequency, and impedance versus frequency. In total thirty-six tests were conducted.

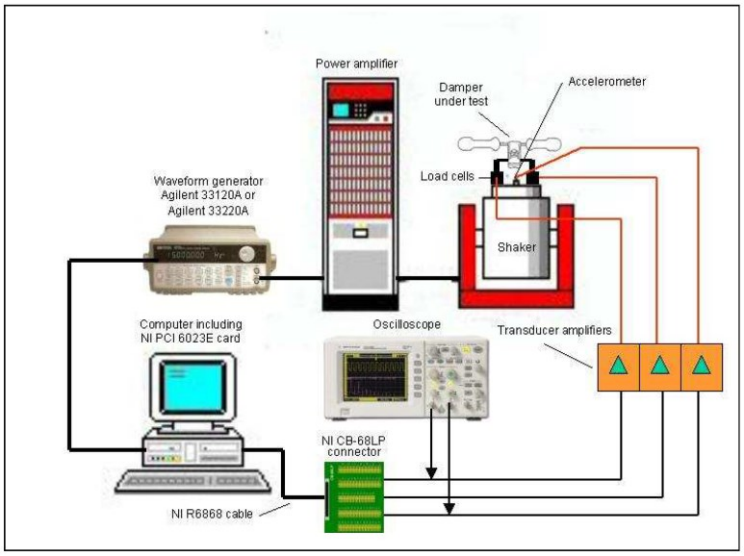

Figure 5: The layout of the test stand used for evaluating the dynamic response of dampers at the VIP Damper Test facility.

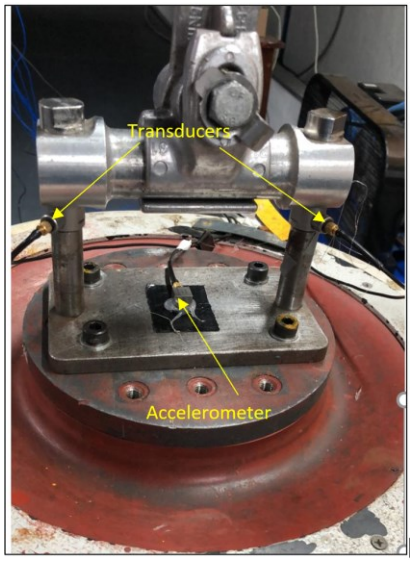

Figure 6: The accelerometer stuck on the base of the shaker and two two force transducers stuck on both sides of the jig

2.3 Analytical model

Figure 7 presents a comprehensive, physical representation at full scale of the vibration damper.. However, due to its large size, developing a comprehensive mathematical model for the entire damper is challenging. To streamline the computational process, a half-scale model of the damper is utilized, as depicted in Figure 8 [17]. This half model utilizes three coordinate systems, labeled as O_1, O_2, and O_3. The configuration is treated as consisting of three beams and three masses. The initial coordinate system, O_1, is situated at the clamp, with mass M_1 positioned at the far end. The second and third coordinate systems are located on either side of the mass M_1, with masses M_2 and M_3 positioned at their respective extreme ends. Mass M_1 is assumed to have rotational degrees of freedom about an axis perpendicular to the length of the messenger cable, while masses M_2 and M_3 are treated as point masses. The vibration displacement along the j coordinate is denoted as Y_1, Y_2 and Y_3, corresponding to the first, second, and third coordinate systems, respectively.

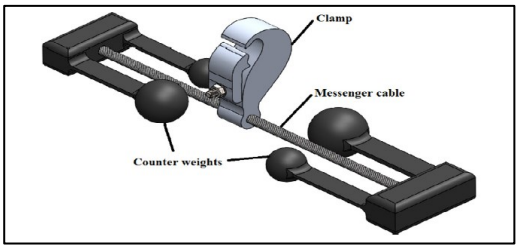

Figure 7: Vibration damper (Vaja et al., 2018).

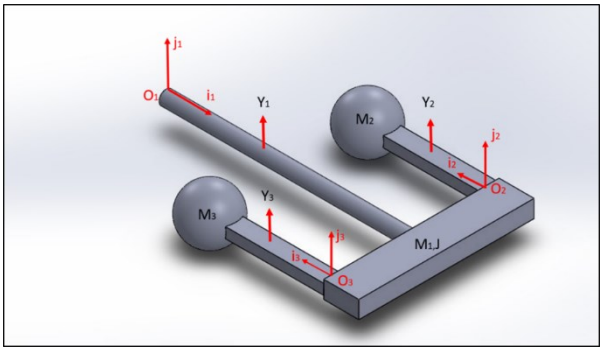

Figure 8: Schematic of the half model of Vibration damper [17]

In developing the analytical model, the equations presented in Appendix A from Eqs (1) to (11) by Vaja et al. (2018, p. 712) were utilized. The potential and kinetic energy of the system can be expressed through Eqs. (1) and (2) respectively.

In Eqs. (1) and (2) from Appendix A, primes denote derivation concerning x, while dots signify derivation concerning time. E represents Young's modulus, and I_1, I_2, and I_3 stand for the area moment of inertia of the messenger cable and beams, respectively. J denotes the rotational inertia of the mass M_1, $L_1$is the length, and m_1 is the mass per unit length of the cable. $L_2$and L_3represent the lengths, and m_2 and $m_3$are the mass per unit length of the

beams, respectively. By employing Hamilton's principle, the system's equations of motion are derived, Eqs. (3), (4), and (5). If the system is considered to exhibit harmonic motion, Eqs. (6), (7), and (8) can be formulated as shown in Appendix A. There, ω represents the natural frequency, and the configurations of the modes are specified in Eqs. (9), (10), and (11).

Vaja et al. (2018, p. 712) applied the boundary conditions, and the characteristic equation was derived by imposing the specified boundary conditions on the general solution. This process results in the formulation of twelve simultaneous equations that are homogeneous, which are then organized to construct the coefficient matrix detailed in Appendix B Eq. (12). The characteristic equation is subsequently obtained by setting the determinant of the coefficient matrix equal to zero.

3 RESULTS AND DISCUSSION

This section discusses the results of the three methods that have been used to conduct experiments.

3.1 Experimental Results and Discussion for Puma System

Drawing from the initial findings of the investigation concerning the asymmetric damper, it was observed that the damper exhibits four degrees of freedom and possesses the potential to generate additional resonance frequencies through modification [19, 20]. The frequency versus acceleration graphs presented in Figures 9, 10, 11, 12, 13, and 14 show the outcomes of experiments where different masses were introduced to the inner parts from damper number 1 to damper number 6.

Points 1,2 3 and 4 in Figure 9 show the results of an asymmetric damper with no additional masses added to the inner parts of the bigger and smaller weights of the damper. Points 3 and 4 in Figure 9 on the graph represent the inner parts of the bigger and smaller weights of the damper. The two lines at points 3 and 4 are approximately the same at the same peak point, showing there are no added masses on the damper and there is no rotational motion on them. The asymmetric damper confirms that it is a four-degree of freedom or 4R [1, 2]. The findings indicated that a Stockbridge damper with an asymmetric design can dampen four different resonance frequencies.

In Figures 10 to 14, points 1 to 6 on each graph correspond to resonance frequencies resulting from the modified damper. Points 1, 2, 4, and 6 on the graphs represent resonance frequencies inherent to the asymmetric damper, whereas points 3 and 5 indicate resonance frequencies attributed to the additional masses. These findings demonstrate that the modified asymmetric damper when augmented with two alternating masses, can generate six resonance frequencies [19]. This aligns with the observations made by other researchers in their study of the modeling and analysis of a vibration absorber designed for overhead power lines using simulation methods [17]. Consequently, the modified asymmetric damper can be classified as a six-degree-of-freedom system. The findings indicated that a modified Stockbridge damper design can dampen six different resonance frequencies [19]. The number of resonance frequencies produced by the damper is a critical factor in its effectiveness. A higher number of resonance frequencies indicates that the damper can target or counteract a broader range of vibrational frequencies produced by the overhead power lines. This suggests that the modified damper is designed to be more effective in reducing the amplitude of vibrations in the power

lines in cases where other frequencies are present. The most important part observed was that the bandwidths of the modified damper were shorter than the bandwidths of the damper producing four resonance frequencies. The additional frequencies are quite low which is a good result as they can apply to a larger range of power lines

The acceleration increases as the additional masses are introduced to the damper. If the acceleration of the modified damper increases, it suggests that the damper absorbs more energy. The resultant force equals the product of the mass being accelerated and the acceleration ($F_{resultant}$ = ma) [21]. In the context of vibration damping, this could indicate that the modified damper is more effective at dissipating energy from the vibrating system. A higher acceleration typically implies that more force is being exerted on the damper, which, in turn, means that the damper is absorbing more energy from the vibrations of overhead power lines. This increased absorption of energy suggests that the modified damper is effectively dissipating energy, which is crucial for reducing the amplitude of vibrations in the overhead power lines and improving system stability.

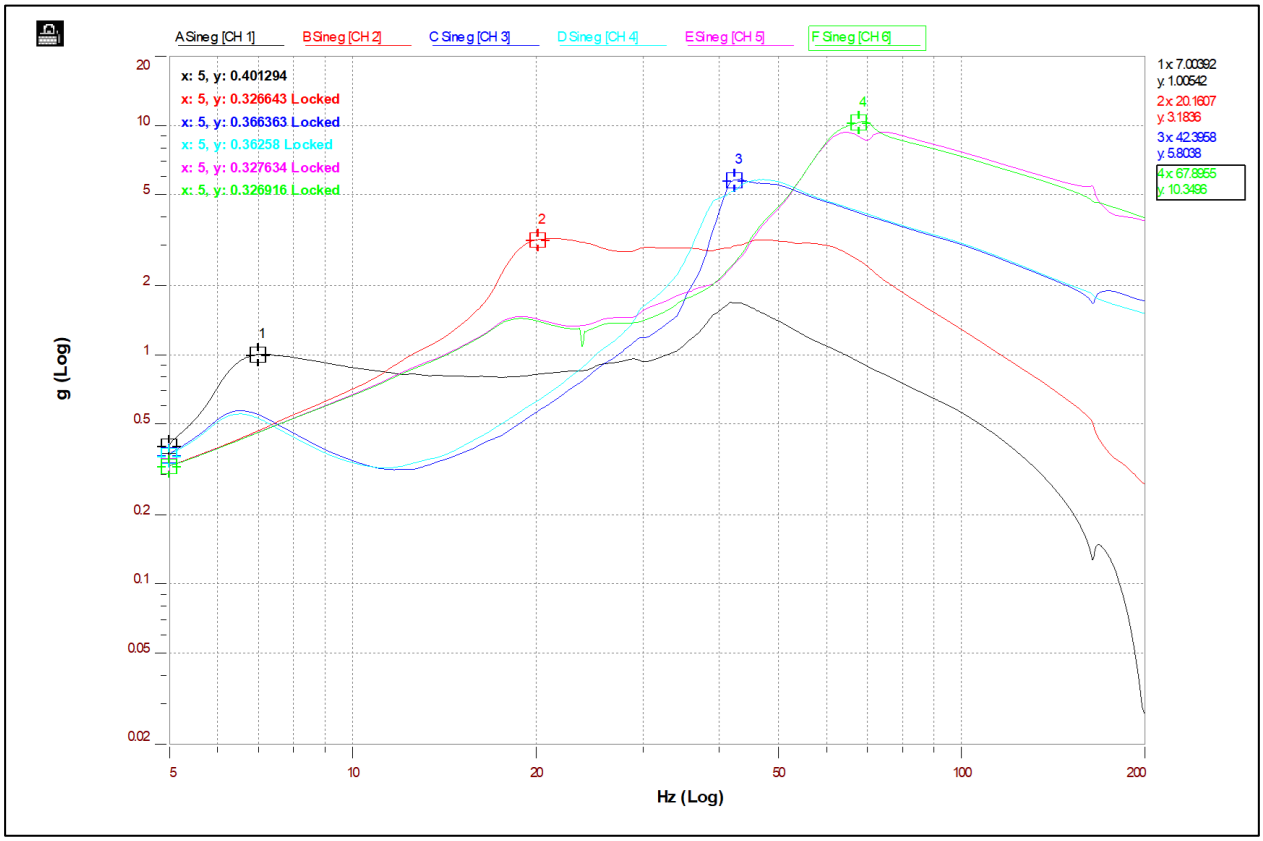

Figure 9: The damper with no added masses

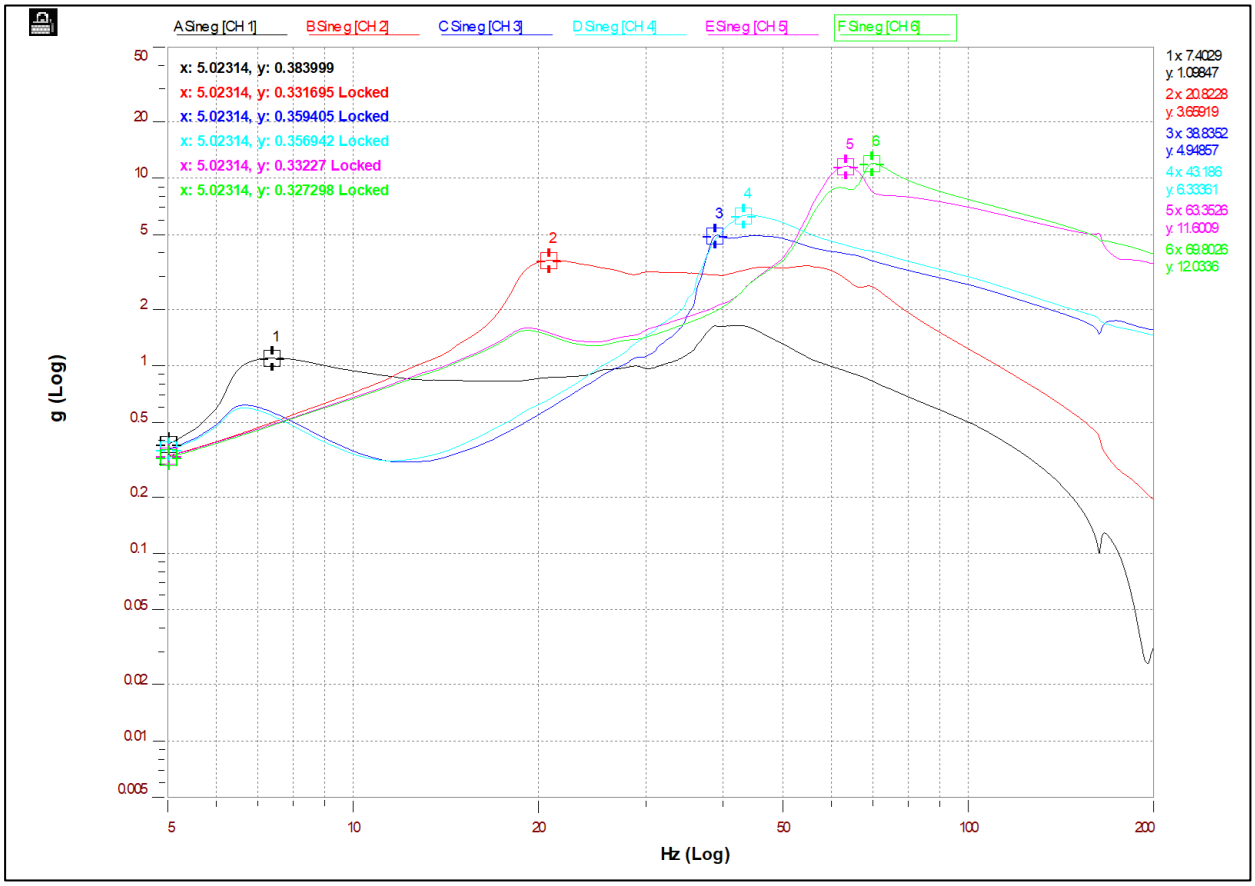

Figure 10: The damper with masses of 10 and 20 grams added to it.

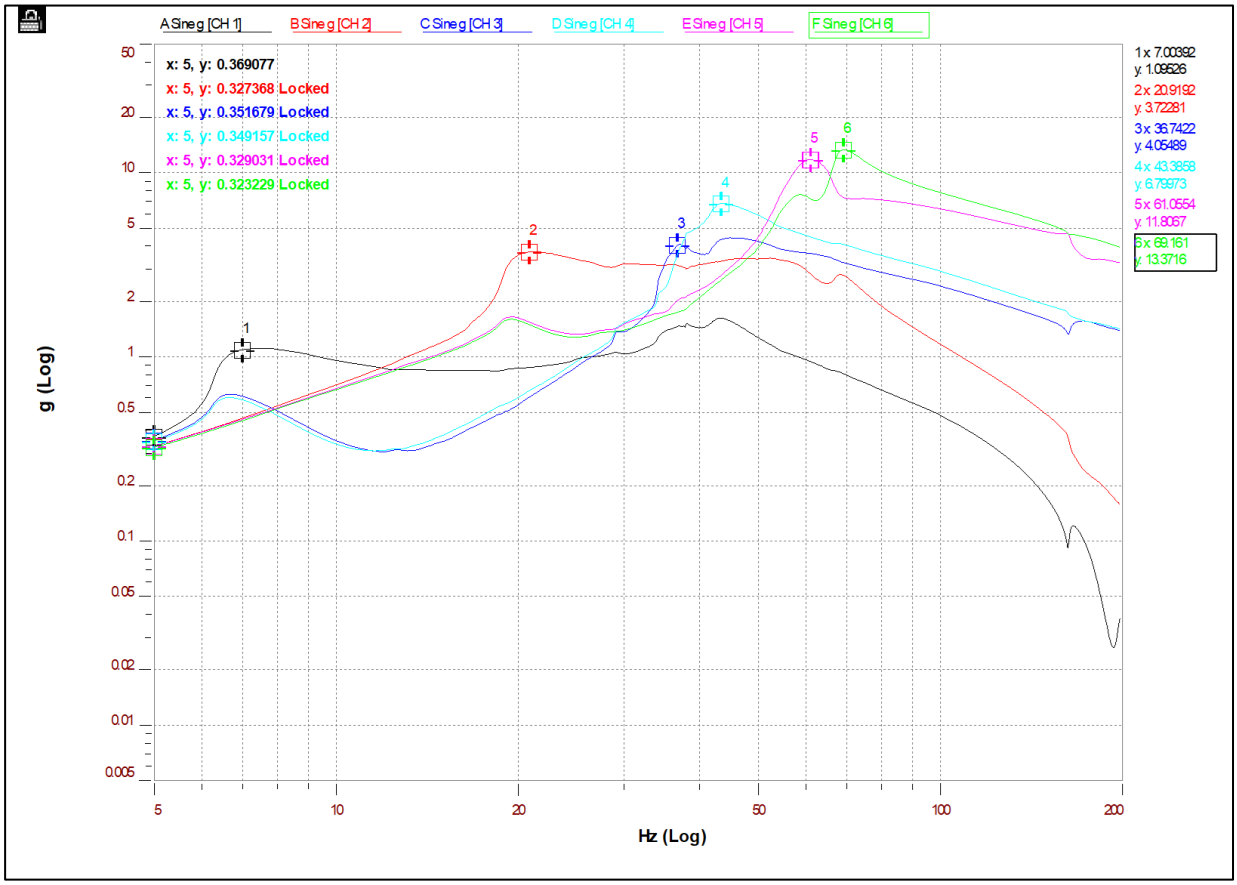

Figure 11: The damper with masses of 25 g and 50 g added to it.

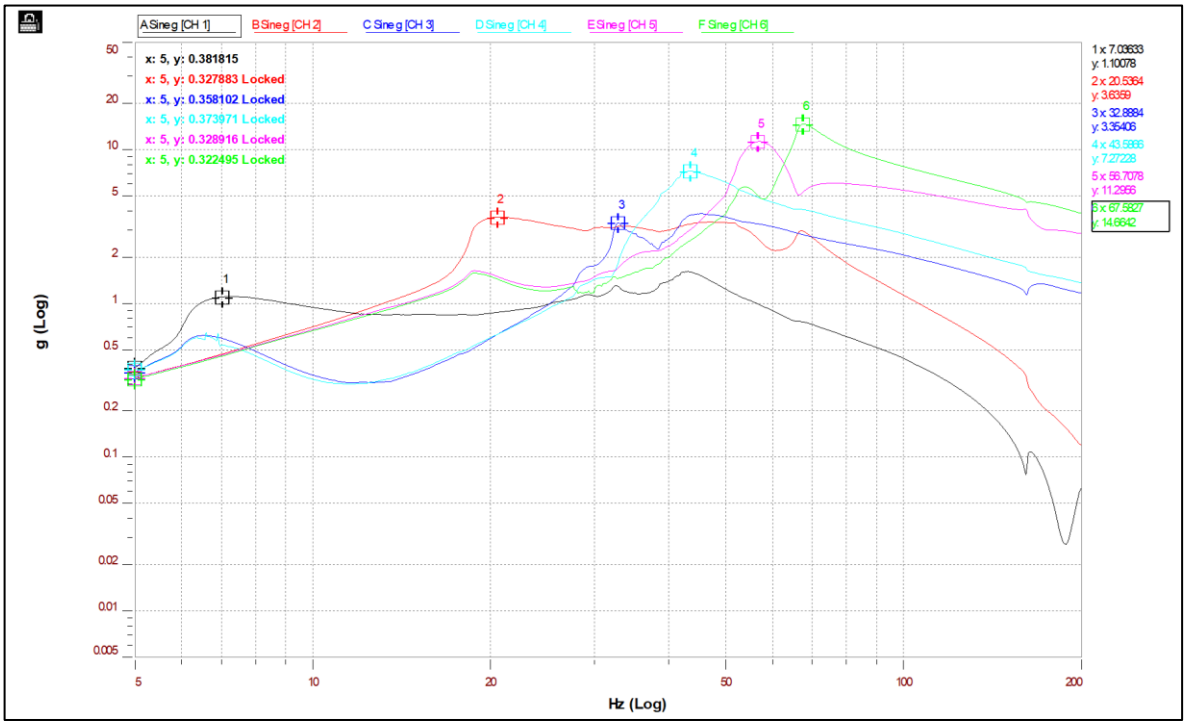

Figure 12: The damper with masses of 50 and 100 grams added to it.

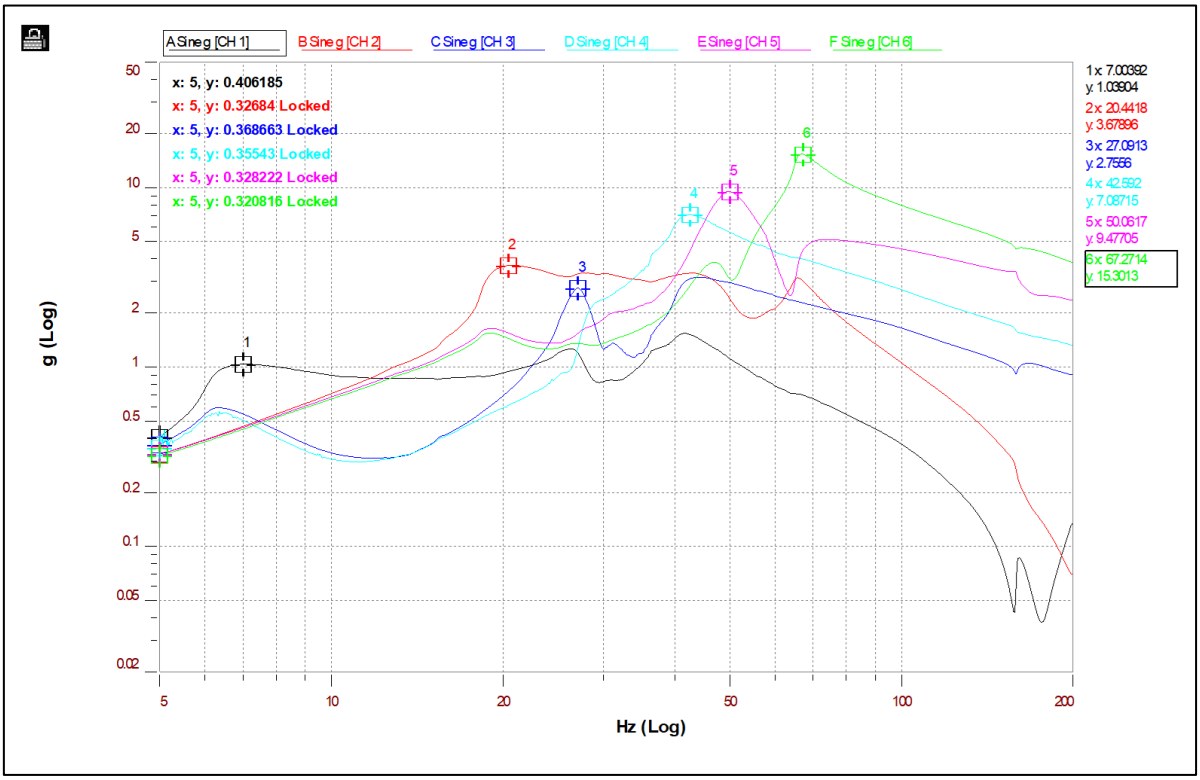

Figure 13: The damper with masses of 100 and 200 grams added to it.

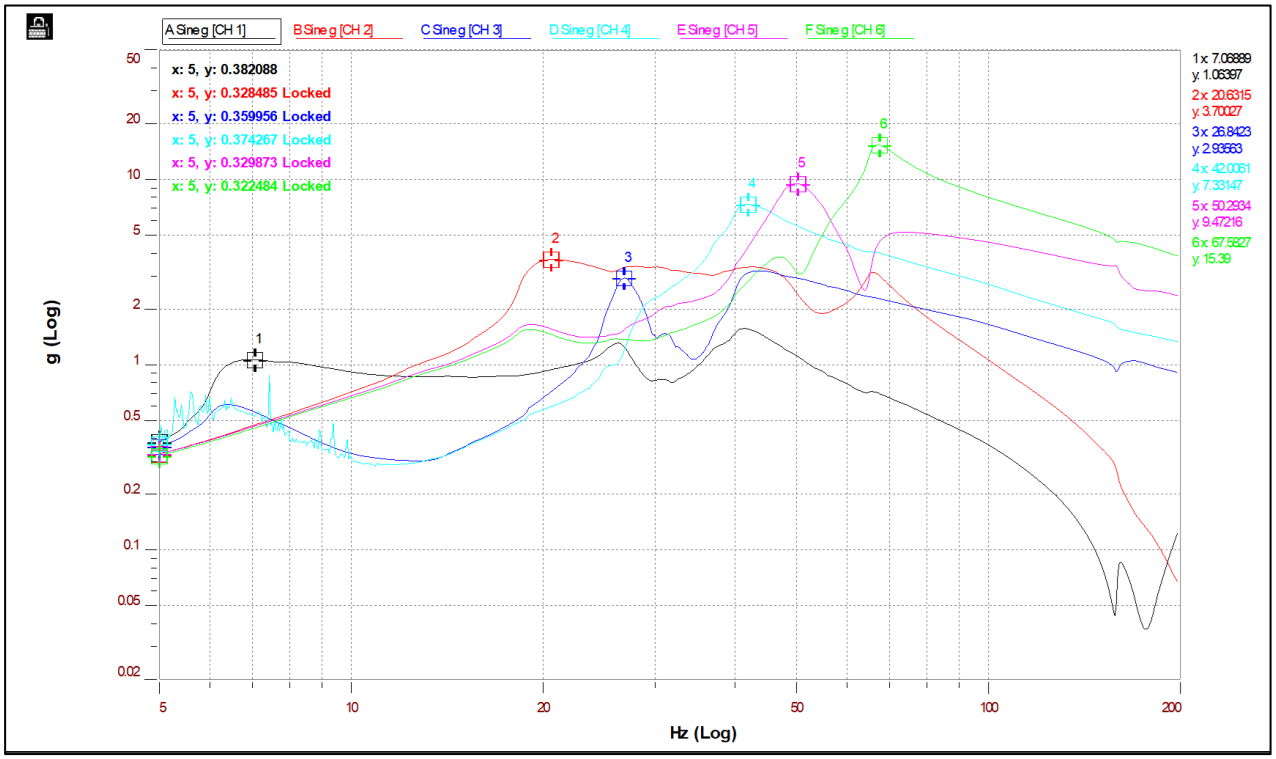

Figure 14: The damper with masses of 120 and 230 grams added to it.

3.2 Experimental Results and Discussion for VIP (Vibration Isolation Platform)

The graphs of forces, powers, and impedances versus frequencies for damper number one to damper number six are presented in Figures 15 to 32. The force is imparted by the electrodynamic shaker to the damper. This force causes the damper to move and respond to the vibrations. The power is imparted on the damper by the electrodynamic shaker which is the rate at which the shaker does work on the damper. Impedance of the damper can be measured by applying a known force and measuring the resulting velocity. Two tests were conducted for each damper

To summarize the results of Damper numbers 1 to 6, there is a noticeable change produced by the addition of different sizes of masses to each inner part of the dampers. The resonance frequencies generated by the dampers vary as different masses are incrementally added to each internal part of the damper during testing Table 2 shows the count of resonance frequencies generated by each damper. The graphs of force, power, and impedance versus frequency for the damper numbers 3 and 4 show the increase in the count of resonance frequencies generated compared to the other dampers tested. Power is equal to the product of force and velocity (Power = Force x Velocity) [21]. Each point of resonance frequency produced leads to the power that could be absorbed and dissipated by the damper from

overhead transmission lines [22]. The damper numbers 3 and 4 seem to be optimal dampers for the test conducted. They performed particularly well or demonstrated desirable characteristics during the conducted tests.

The impedance is a measure of the damper's resistance to the movement or transmission of vibrations within transmission lines [14, 22, 23]. This resistance is crucial for reducing the impact of vibrations and ensuring the stability and reliability of the transmission lines. Standard Stockbridge dampers undergo design considerations to closely align their mechanical impedance with the optimal damper impedance identified for the cable under protection [14, 22, 23]. As explained, the number of resonance frequencies produced by damper numbers 3 and 4 in the impedance graphs is more than the number of resonance frequencies produced by damper 1, 2, 5, and 6 tested. This suggests their higher effectiveness in reducing vibration compared to the latter group.

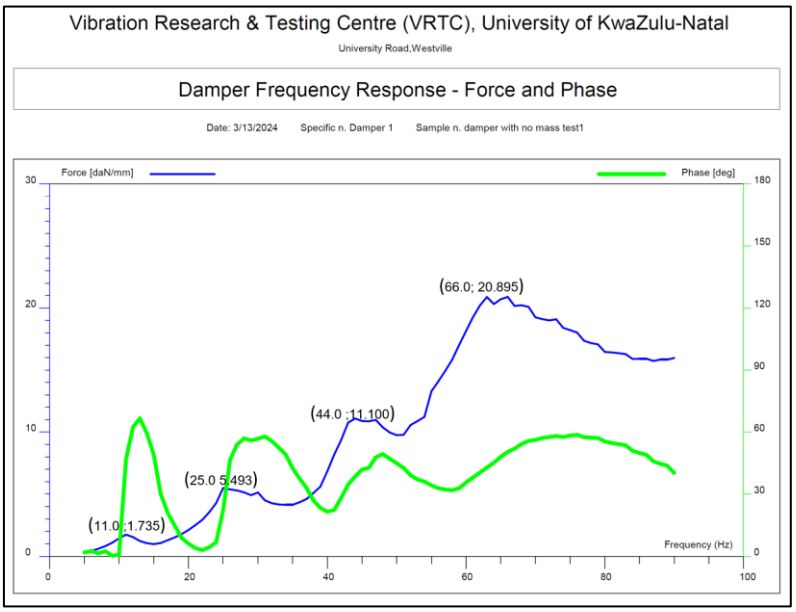

Figure 15: The graph of force vs frequency for damper number 1

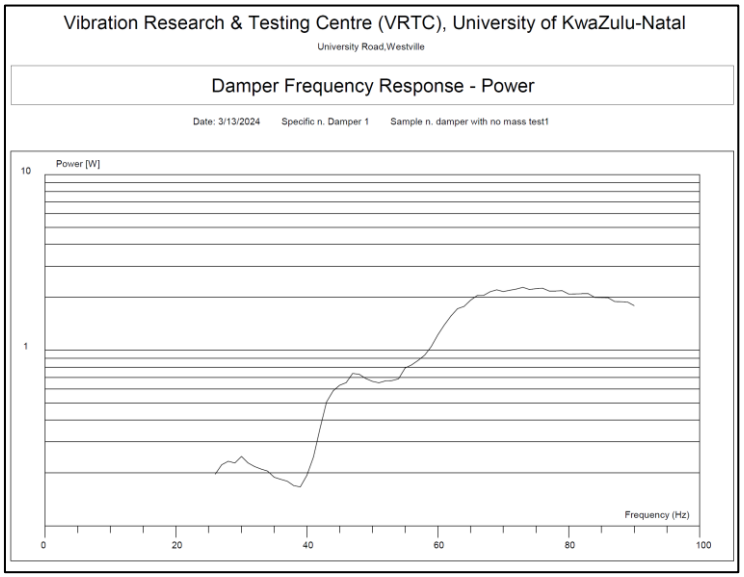

Figure 16: The graph of power vs frequency for damper number 1

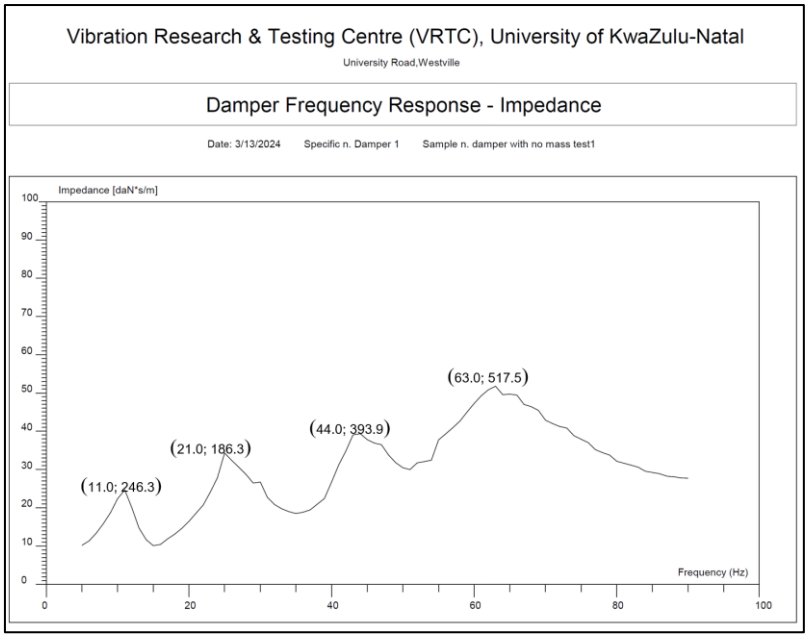

Figure 17: The graph of impedance vs frequency for damper number 1

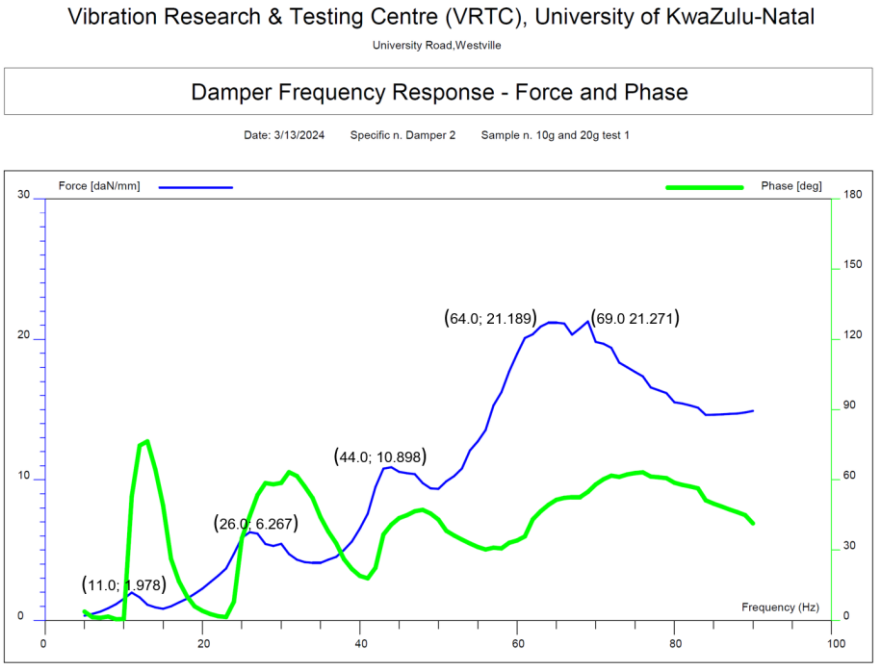

Figure 18: The graph of force vs frequency for damper number 2

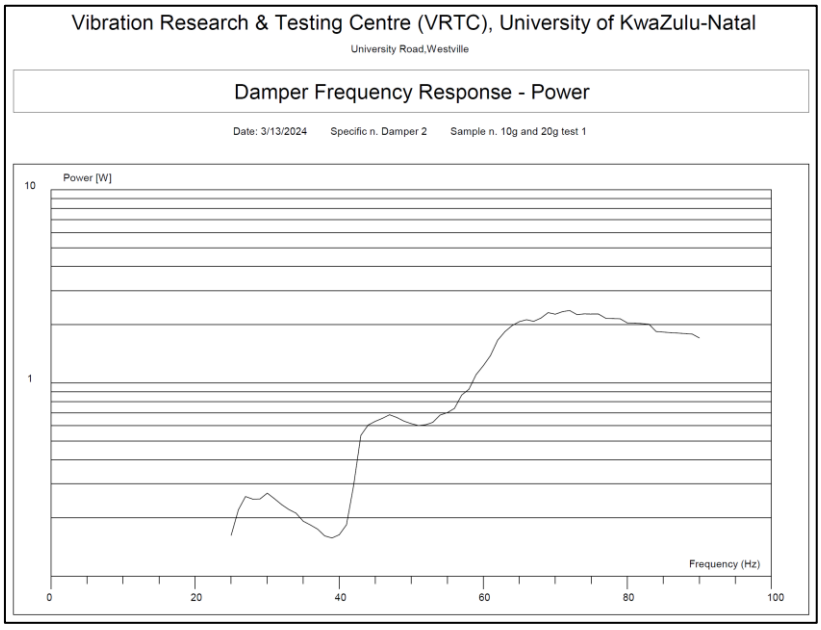

Figure 19: The graph of power vs frequency for damper number 2

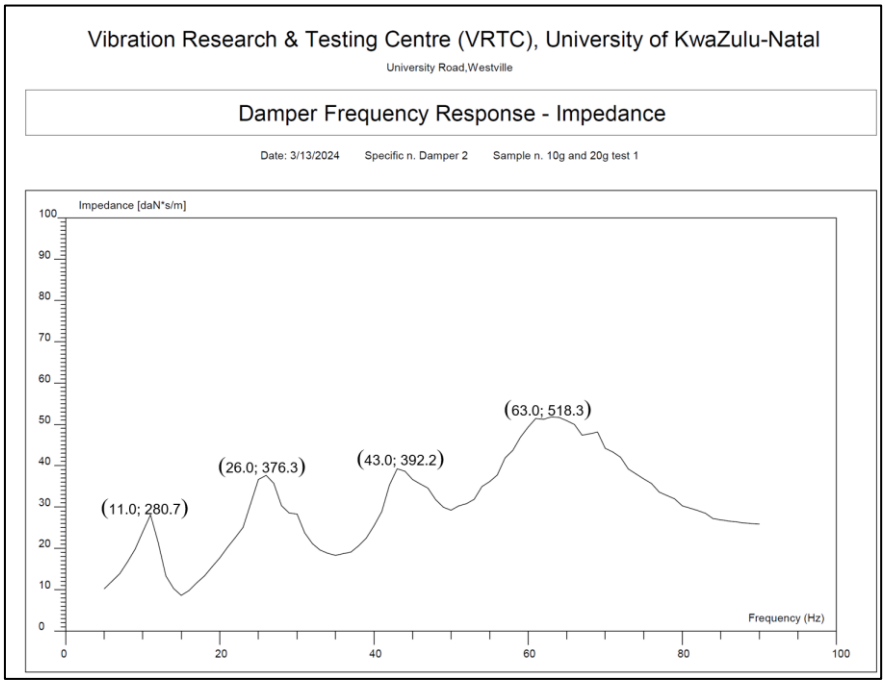

Figure 20: The graph of impedance vs frequency for damper number 2

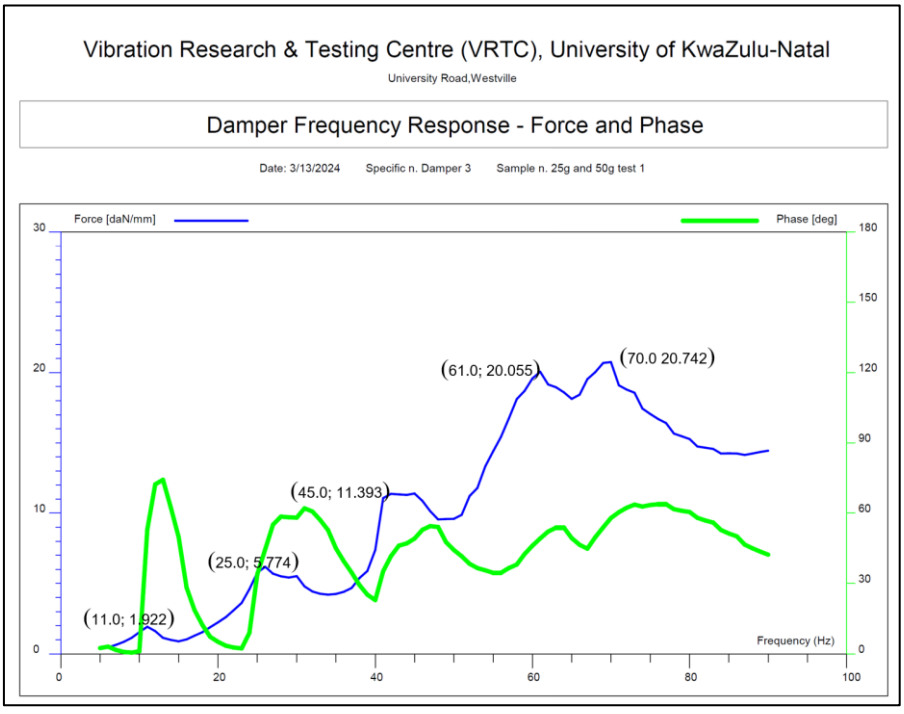

Figure 21:: The graph of force vs frequency for damper number 3

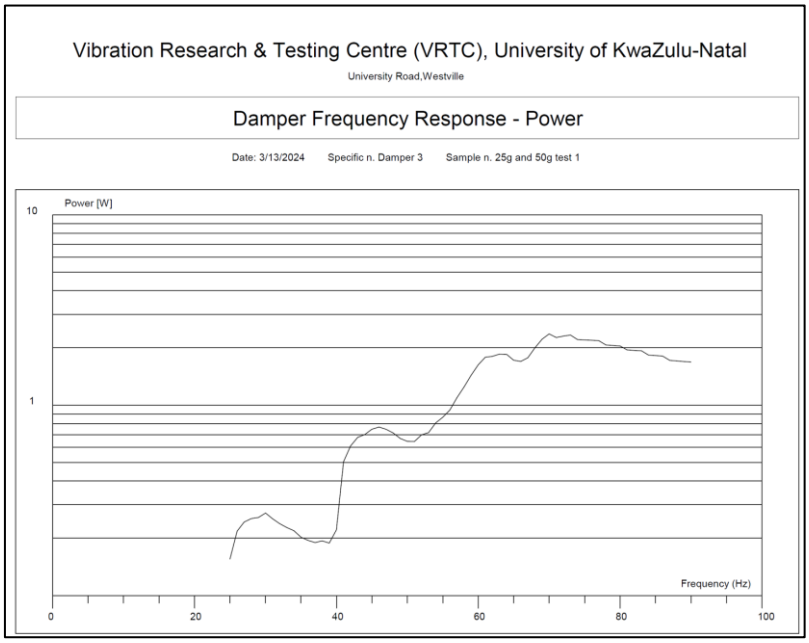

Figure 22: The graph of power vs frequency for damper number 3

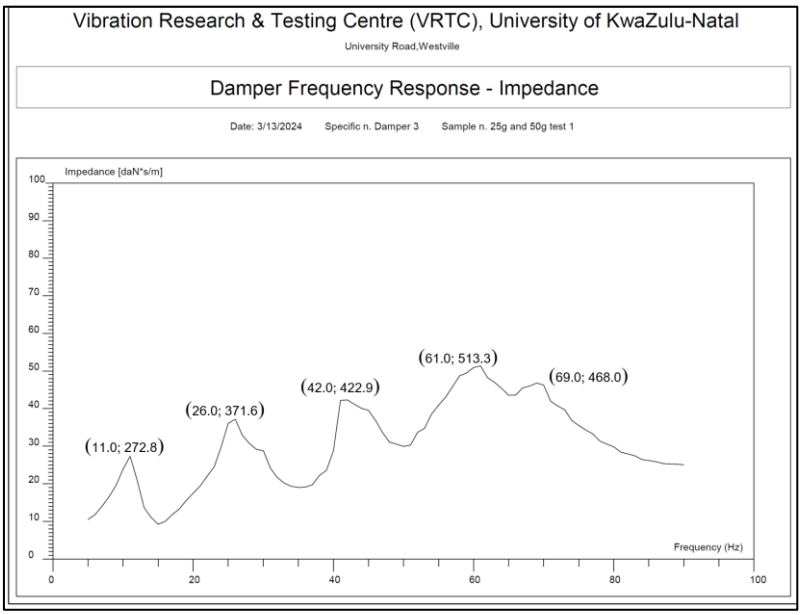

Figure 23: The graph of impedance vs frequency for damper number 3

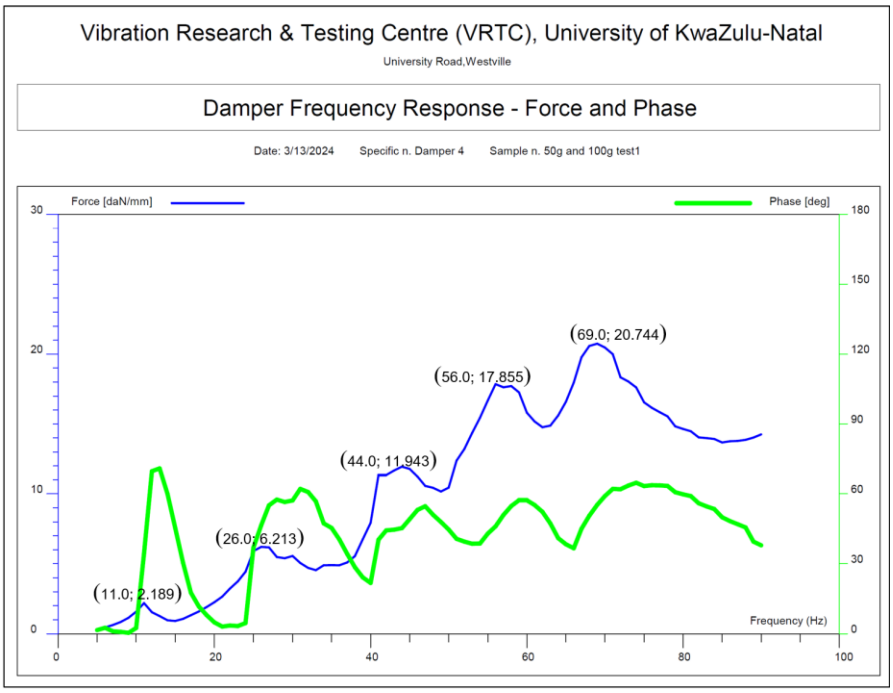

Figure 24: The graph of force vs frequency for damper number 4

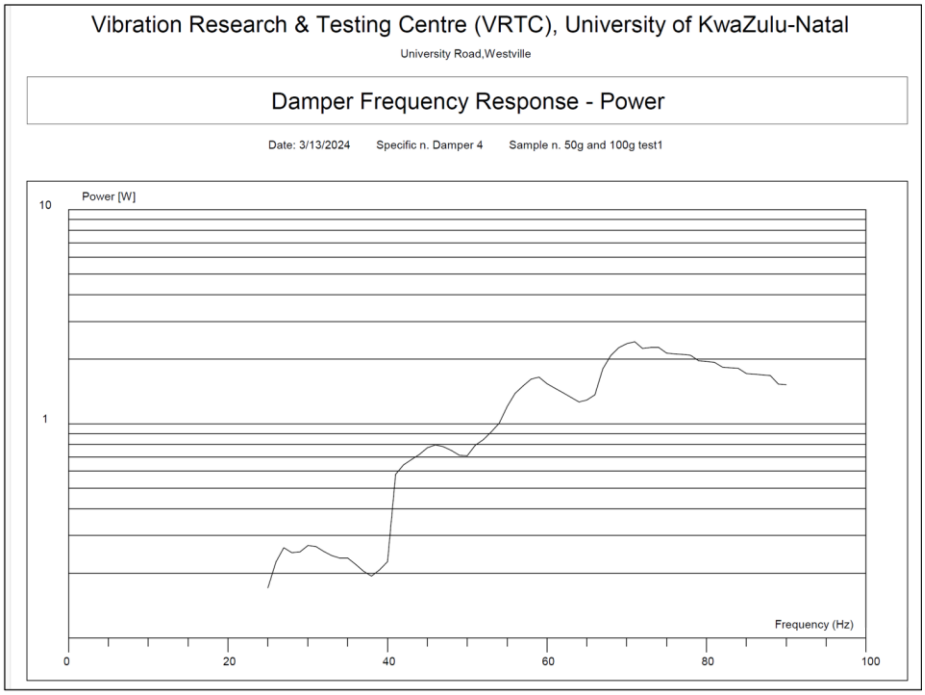

Figure 25: The graph of power vs frequency for damper number 4

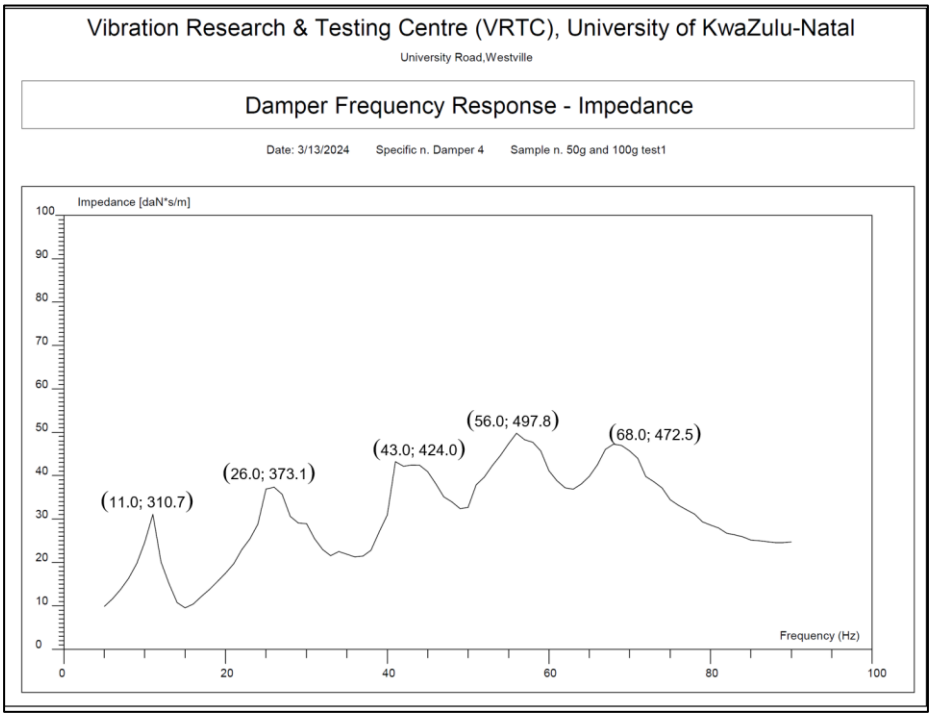

Figure 26: The graph of impedance vs frequency for damper number 4

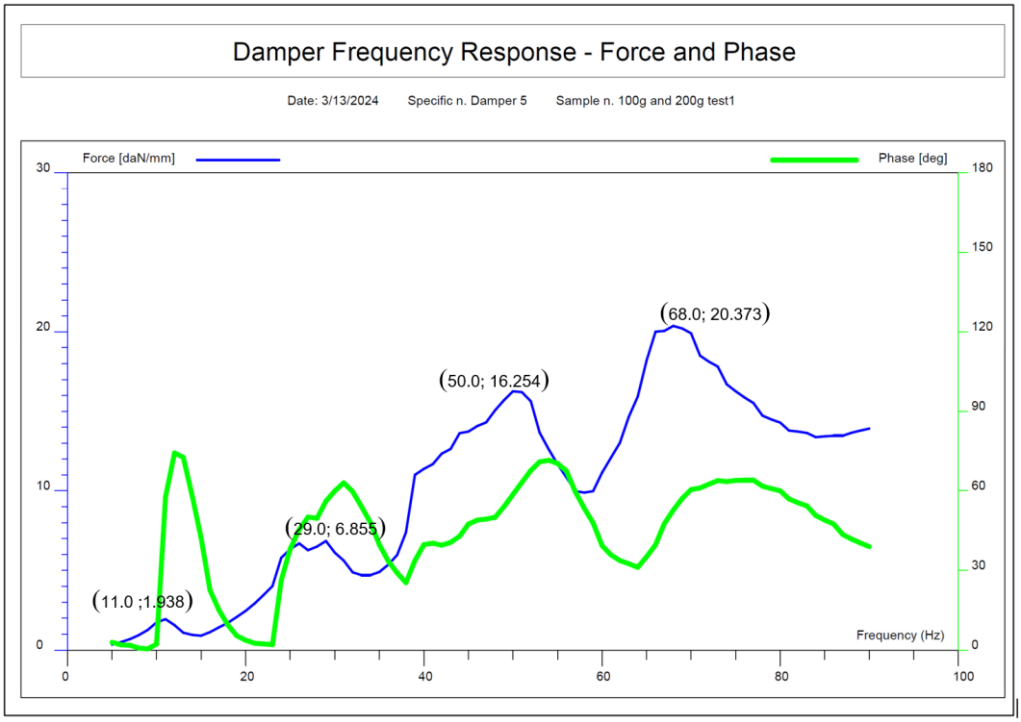

Figure 27:: The graph of force vs frequency for damper number 5

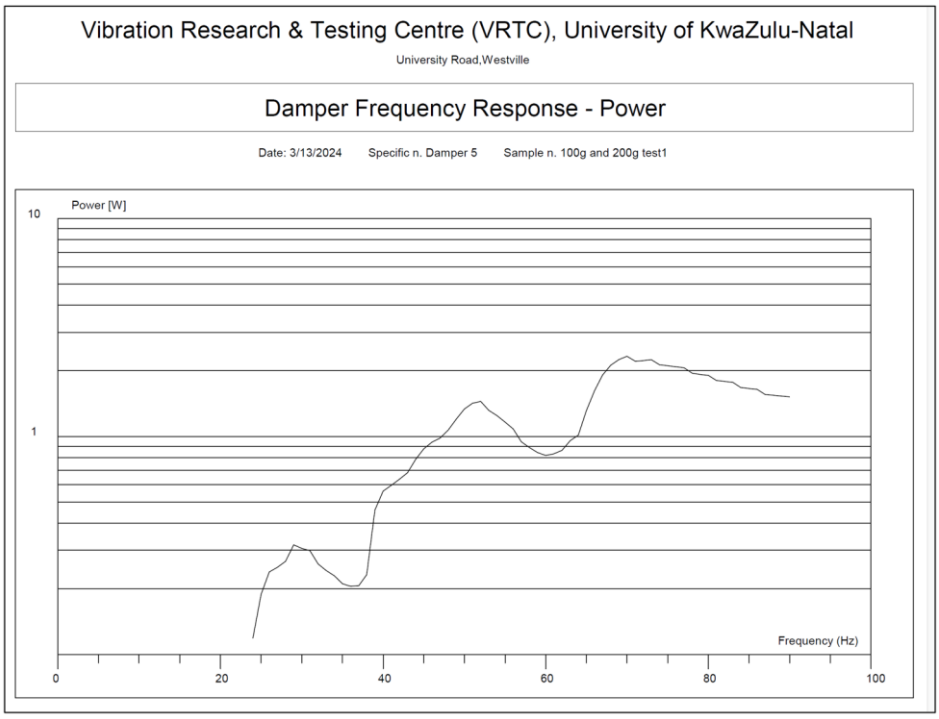

Figure 28: The graph of power vs frequency for damper number 5

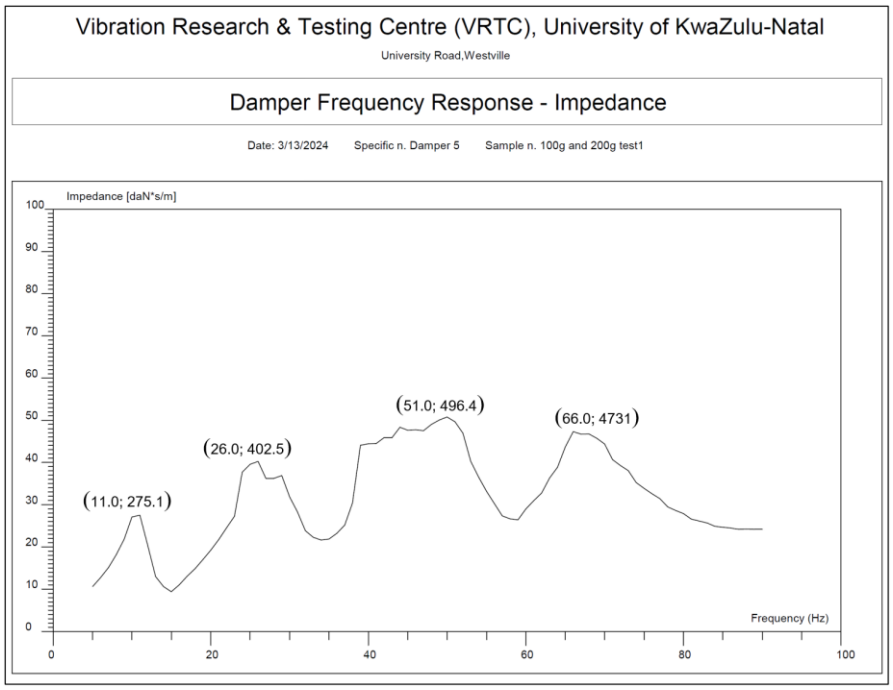

Figure 29: The graph of impedance vs frequency for damper number 5

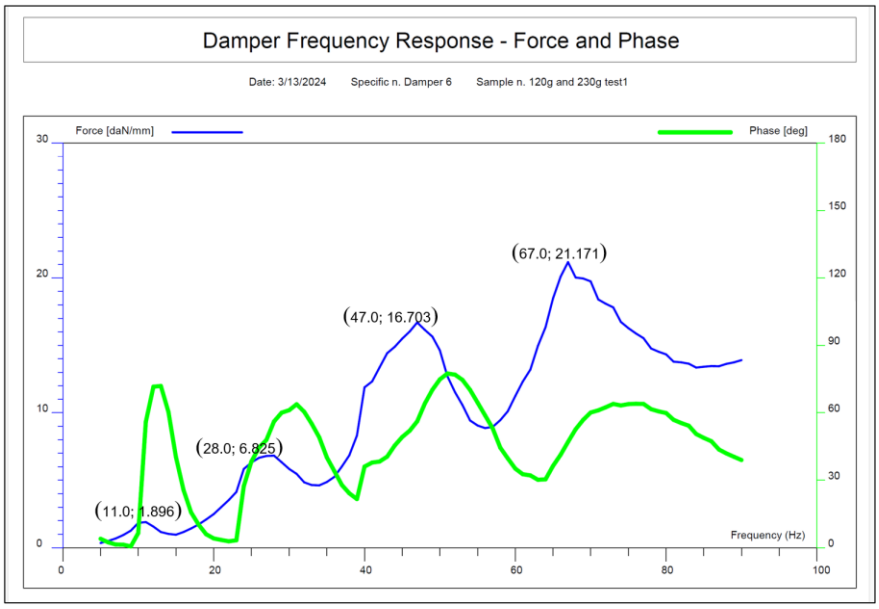

Figure 30: The graph of force vs frequency for damper number 6

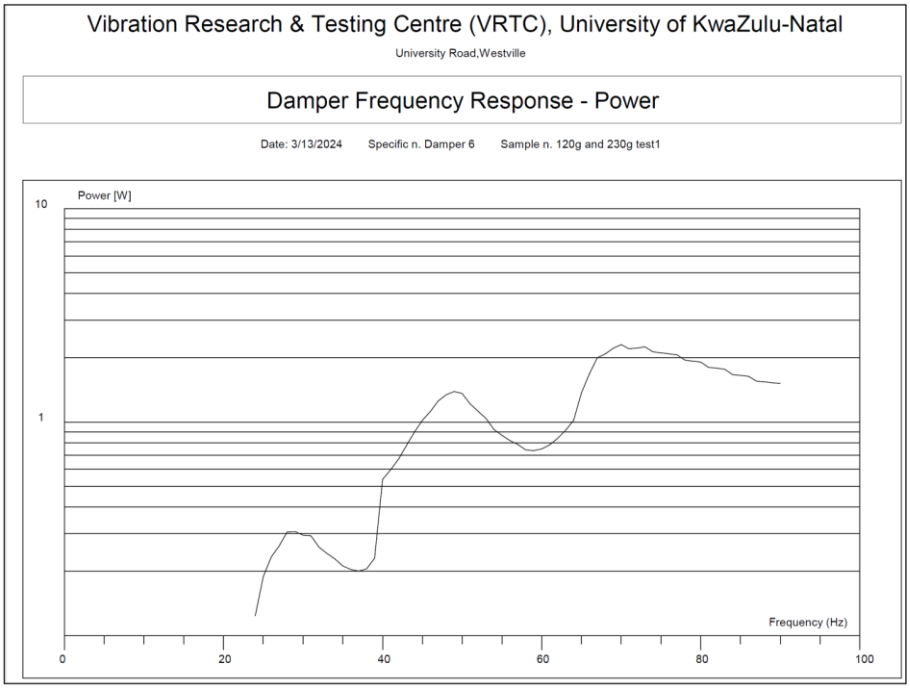

Figure 31: The graph of power vs frequency for damper number 6

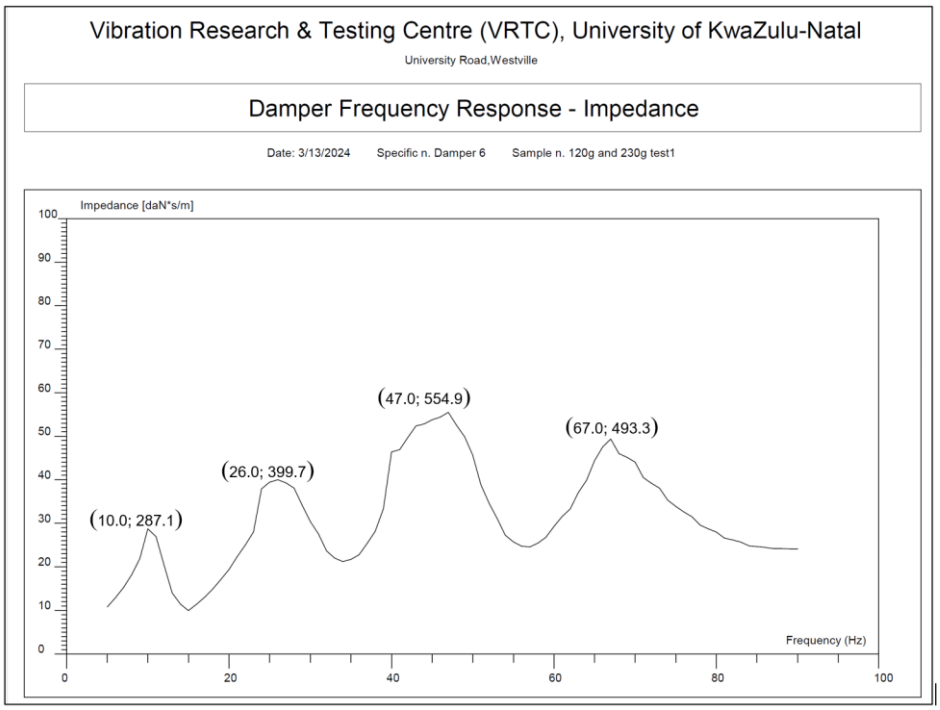

Figure 32: The graph of impedance vs frequency for damper number 6

Table 2: Number of resonance frequencies produced by each damper during the tests conducted

Damper numbers	Masses on the smaller weight in grams	Masses on the bigger weight in grams	Number of resonances produced by the graph of force	Number of resonances produced by the graph of power	Number of resonances produced by the graph of impedance
1	0	0	4	3	4
2	10	20	4	3	4
3	25	50	5	4	5
4	50	100	5	4	5
5	100	200	4	3	4
6	120	230	4	3	4

3.3 Experimental Results and Discussion for Analytical Model

The determination of the resonance frequencies of the vibration damper was carried out using the analytical model. To validate these results, the experimental model was employed. Tables 3 offer a comparison of the resonance frequencies acquired from both methodologies. The maximum variation observed was 3,194 %. Both models confirm that the new vibration

damper exhibits six resonant frequencies within the Aeolian vibration frequency range. This represents a significant increase in the number of resonant frequencies compared to the conventional Stockbridge damper, which has four resonant frequencies. This represents a 50% increase in resonant frequencies. Since energy is absorbed at resonant frequencies, this increase suggests improved effectiveness of the damper.

Good agreement was observed between experimental and analytical model results, except for one data point where the percentage error was -16,4667 %. The derivation ranged from 0,165766 % to 3,194013% for the percentage error in the range from 20.5973 to 65.4241 Hz (Analytical Model results). This indicates that the model performs well for higher frequencies rather than low frequencies. It must be noted that the analytical model developed by Vaja et al., (2018) was not forced vibration, it was developed based on free vibrations. The electromagnetic shaker applied a force to the modified asymmetric Stockbridge damper during the conduction of experiments, meaning it was a forced vibration system

Table 3: Resonance frequency of the experimental model and the analytical model of the Vibration using damper number 6

Added masses of 120 and 230 g on the damper			
Modes	**Experimental natural frequency (Hz)**	**Analytical Model results (Hz)**	**Percentage error (%)**
1	7.06889	8.2329	-16,4667
2	20.6315	20.5973	0,165766
3	26.8423	26.4511	1,457401
4	42.0061	40.8910	2,654614
5	50.2934	48.8279	2,913901
6	67.5827	65.4241	3,194013

4 CONCLUSION

The results showed that it is possible to build a prototype damper with an increased number of resonance frequencies than the current damper producing four resonance frequencies. Previous research has indicated that modifying the counterweight design could optimize resonant frequencies. Consequently, a new vibration damper could be developed. The paper presented an analytical model for the vibration damper, and the analytical model's outcomes were verified through an experimental model. Resonant frequencies of the asymmetric damper were determined using experimental data. The findings demonstrated a distinct rise in resonant frequencies with the new design, signifying superior damping performance compared to the conventional Stockbridge damper. The unique vibration damper's geometric features can be further adjusted to attain improved damping and resonance characteristics. The paper is in support of the research conducted by Vaja et al., (2018).

Appendix A

$$T = \frac{1}{2} m_1 \int_0^{L_1} \dot{Y}_1{}^2 (x_1, t)\, dx + \frac{1}{2} M_1 \dot{Y}_1{}^2 (L_1, t) + J\dot{Y}_1' (L_1, t) + \frac{1}{2} m_2 \int_0^{L_2} \dot{Y}_2{}^2 (x_2, t)\, dx + \frac{1}{2} M_2 \dot{Y}_2{}^2 (L_2, t) + \frac{1}{2} m_3 \int_0^{L_3} \dot{Y}_3{}^2 (x_3, t)\, dx + \frac{1}{2} M_3 \dot{Y}_3{}^2 (L_3, t) \quad (1)$$

$$V = \frac{1}{2} EI_1 \int_0^{L_1} Y''^2 (x_1, t)\ dx + \frac{1}{2} EI_2 \int_0^{L_2} Y''^2 (x_2, t)\ dx + \frac{1}{2} EI_3 \int_0^{L_3} Y''^2 (x_3, t)\ dx \quad (2)$$

$$m_1 \ddot{Y}_1 = -EI_1 Y_1^{IV} \quad (3)$$

$$m_2 \ddot{Y}_2 = -EI_2 Y_2^{IV} \quad (4)$$

$$m_3 \ddot{Y}_3 = -EI_3 Y_3^{IV} \quad (5)$$

$$Y_1(x_1, t) = F(x_1) e^{i\omega t} \quad (6)$$

$$Y_2(x_2, t) = G(x_2) e^{i\omega t} \quad (7)$$

$$Y_3(x_3, t) = H(x_3) e^{i\omega t} \quad (8)$$

$$F(x_1) = a_1 \sin \beta_1 x_1 + a_2 \cos \beta_1 x_1 + a_3 \sinh \beta_1 x_1 + a_4 \cosh \beta_1 x_1 \quad (9)$$

$$G(x_2) = a_5 \sin \beta_2 x_2 + a_6 \cos \beta_2 x_2 + a_7 \sinh \beta_2 x_2 + a_8 \cosh \beta_2 x_2 \quad (10)$$

$$H(x_3) = a_9 \sin \beta_3 x_3 + a_{10} \cos \beta_3 x_3 + a_{11} \sinh \beta_3 x_3 + a_{12} \cosh \beta_3 x_3 \quad (11)$$

Appendix B

(12)

$$\begin{bmatrix} A_1 & 0 & A_3 & 0 & 0 & 0 & 0 & 0 & 0 & 0 & 0 & 0 \\ 0 & B_2 & 0 & B_4 & 0 & 0 & 0 & 0 & 0 & 0 & 0 & 0 \\ C_1 & C_2 & C_3 & C_4 & C_5 & 0 & C_7 & 0 & 0 & 0 & 0 & 0 \\ D_1 & D_2 & D_3 & D_4 & 0 & D_6 & 0 & D_8 & 0 & 0 & 0 & 0 \\ E_1 & E_2 & E_3 & E_4 & E_5 & 0 & 0 & 0 & E_9 & 0 & E_{11} & 0 \\ F_1 & F_2 & F_3 & F_4 & 0 & 0 & 0 & 0 & 0 & F_{10} & 0 & F_{12} \\ G_1 & G_2 & G_3 & G_4 & G_5 & 0 & G_7 & 0 & F_9 & 0 & F_{11} & 0 \\ H_1 & H_2 & H_3 & H_4 & 0 & H_6 & 0 & H_8 & 0 & H_{10} & 0 & H_{12} \\ 0 & 0 & 0 & 0 & I_5 & I_6 & I_7 & I_8 & 0 & 0 & 0 & 0 \\ 0 & 0 & 0 & 0 & J_5 & J_6 & J_7 & J_8 & 0 & 0 & 0 & 0 \\ 0 & 0 & 0 & 0 & 0 & 0 & 0 & 0 & K_9 & K_{10} & K_{11} & K_{12} \\ 0 & 0 & 0 & 0 & 0 & 0 & 0 & 0 & L_9 & L_{10} & L_{11} & L_{12} \end{bmatrix} \cdot \begin{bmatrix} a_1 \\ a_2 \\ a_3 \\ a_4 \\ a_5 \\ a_6 \\ a_7 \\ a_8 \\ a_9 \\ a_{10} \\ a_{11} \\ a_{12} \end{bmatrix} = 0$$

Where

$$A_1 = 1; A_3 = 1$$

$$B_2 = 1; B_4 = 1$$

$$C_1 = \sin \beta_1 L_1 \, ; C_2 = \cos \beta_1 \, L_1;$$

$$C_3 = \sinh \beta_1 L_1 \, ; C_4 = \cosh \beta_1 \, L_1$$

$$C_5 = \beta_2; C_7 = \beta_2$$

$$D_1 = \sin \beta_1 L_1 \, ; D_2 = \cos \beta_1 \, L_1;$$

$$D_3 = \sinh \beta_1 L_1 \, ; D_4 = \cosh \beta_1 \, L_1$$

$$D_6 = -1; D_8 = -1$$

$$E_1 = \beta_1 \cos \beta_1 \, L_1; \; E_2 = -\beta_1 \sin \beta_1 L_1$$

$$E_3 = \beta_1 \cosh \beta_1 L_1 \; ; \; E_4 = \beta_1 \sinh \beta_1 L_1$$

$$E_9 = \beta_3; \; E_{11} = \beta_3$$

$$F_1 = \beta_1 \sin \beta_1 L_1; \; F_2 = \beta_1 \cos \beta_1 L_1$$

$$F_3 = \beta_1 \sinh \beta_1 L_1 \; ; \; F_4 = = \beta_1 \cosh \beta_1 L_1$$

$$F_{10} = -1; \; F_{12} = -1$$

$$G_1 = -EI_1\beta_1^3 \cos \beta_1 L_1 - M_1\omega^2 \sin \beta_1 L_1 \; ; \; G_2 = EI_1\beta_1^3 \sin \beta_1 L_1 - M_1 \omega^2 \cos \beta_1 L_1$$

$$G_3 = EI_1\beta_1^3 \cosh \beta_1 L_1 - M_1\omega^2 \sinh \beta_1 L_1 \; ; \; G_4 = EI_1\beta_1^3 \sinh \beta_1 L_1 - M_1 \omega^2 \cosh \beta_1 L_1$$

$$G_5 = -EI_2\beta_2^3 \; ; \; G_7 = EI_2\beta_2^3$$

$$G_9 = -EI_3\beta_3^3 \; ; \; G_{11} = EI_3\beta_3^3$$

$$H_1 = -EI_1\beta_1^2 \sin \beta_1 L_1 + J\omega^2 \beta_1 \cos \beta_1 L_1; \; H_2 = -EI_1\beta_1^2 \cos \beta_1 L_1 - J\omega^2 \beta_1 \sin \beta_1 L_1$$

$$H_3 = EI_1\beta_1^2 \sinh \beta_1 L_1 + J\omega^2 \beta_1 \cosh \beta_1 L_1 \; ; \; H_4 = EI_1\beta_1^2 \cosh \beta_1 L_1 + J\omega^2 \beta_1 \sinh \beta_1 L_1$$

$$H_6 = EI_2\beta_2^2 \; ; \; H_8 = EI_2\beta_2^2$$

$$H_{10} = -EI_3\beta_3^2 \; ; \; H_{12} = EI_3\beta_3^2$$

$$I_5 = -\beta_2^2 \cos \beta_2 L_2 \; ; \; I_6 = -\beta_2^2 \sin \beta_2 L_2$$

$$I_7 = \beta_2^2 \cosh \beta_2 L_2 \; ; \; I_8 = \beta_2^2 \sinh \beta_2 L_2$$

$$J_5 = M_2\omega^2 \sin \beta_2 L_2 - \beta_2^3 EI_2 \cos \beta_2 L_2 \; ; \; J_6 = M_2\omega^2 \cos \beta_2 L_2 + \beta_2^3 EI_2 \sin \beta_2 L_2$$

$$J_7 = M_2\omega^2 \sinh \beta_2 L_2 + \beta_2^3 EI_2 \cosh \beta_2 L_2 \; ; \; J_8 = M_2\omega^2 \cosh \beta_2 L_2 + \beta_2^3 EI_2 \sinh \beta_2 L_2$$

$$K_9 = -\beta_3^2 \sin\beta_3 L_3;\ K_{10} = -\beta_3^2 \cos\beta_3 L_3$$

$$K_{11} = \beta_3^2 \sinh\beta_3 L_3\ ; K_{12} = \beta_3^2 \cosh\beta_3 L_3$$

$$L_9 = M_3\omega^2 \sin\beta_3 L_3 - \beta_3^3 EI_3 \cos\beta_3 L_3\ ;\ L_{10} = M_3\omega^2 \cos\beta_3 L_3 + \beta_3^3 EI_3 \sin\beta_3 L_3$$

$$L_{11} = M_3\omega^2 \sinh\beta_3 L_3 + \beta_3^3 EI_3 \cosh\beta_3 L_3\ ;\ L_{12} = M_3\omega^2 \cosh\beta_3 L_3 + \beta_3^3 EI_3 \sinh\beta_3 L_3$$

REFERENCES

[1] J. Chan, *EPRI transmission line reference book: Wind induced-induced conductor motion motion*. Palo Alto, California: Electric Power Research Institute 2006.

[2] J. Chan, D. Havard, C. Rawlins, G. Diana, L. Cloutier, J.-L. Lilien*, et al.*, "EPRI Transmission Line Reference Book: wind-induced Conductor Motion," 2009.

[3] O. Griffin and G. Koopmann, "The vortex-excited lift and reaction forces on resonantly vibrating cylinders," *Journal of Sound and Vibration,* vol. 54, pp. 435-448, 1977.

[4] D. Havard, "Assessment of the Cowal JCT x Longwood TS for vibration control," *Toronto, Ontario,* 2008.

[5] J. Lilien, S. Guérard, and B. Godard, "Power Line Aeolian Vibrations," *Published by University of Liège Department of Electronics, Electricity and Computer Sciences, Liège, Belgium,* 2013.

[6] O. Barry, D. C. Oguamanam, and D. C. Lin, "Aeolian vibration of a single conductor with a Stockbridge damper," *Proceedings of the Institution of Mechanical Engineers, Part C: Journal of Mechanical Engineering Science,* vol. 227, pp. 935-945, 2013.

[7] M. A. Bukhari and O. R. Barry, "Nonlinear vibrations analysis of overhead power lines: A beam with mass–spring–damper–mass systems," *Journal of Vibration and Acoustics,* vol. 140, p. 031004, 2018.

[8] M. Dutkiewicz and M. R. Machado, "Measurements in Situ and Spectral Analysis of Wind Flow Effects on Overhead Transmission Lines," *Sound & Vibration,* vol. 53, 2019.

[9] A. L. Braun and A. M. Awruch, "Aerodynamic and aeroelastic analyses on the CAARC standard tall building model using numerical simulation," *Computers & Structures,* vol. 87, pp. 564-581, 2009.

[10] M. A. Bukhari, O. Barry, and E. Tanbour, "On the vibration analysis of power lines with moving dampers," *Journal of vibration and control,* vol. 24, pp. 4096-4109, 2018.

[11] F. Foti and L. Martinelli, "Hysteretic behaviour of stockbridge dampers: Modelling and parameter identification," *Mathematical Problems in Engineering,* vol. 2018, 2018.

[12] N. Barbieri, M. E. Marchi, M. J. Mannala, R. Barbieri, L. d. S. A. V. Barbieri, and G. d. S. A. V. Barbieri, "Nonlinear dynamic analysis of a Stockbridge damper," *Canadian Journal of Civil Engineering,* vol. 46, pp. 828-835, 2019.

[13] X. Luo, L. Wang, and Y. Zhang, "Nonlinear numerical model with contact for Stockbridge vibration damper and experimental validation," *Journal of Vibration and Control,* vol. 22, pp. 1217-1227, 2016.

[14] D. Sauter and P. Hagedorn, "On the hysteresis of wire cables in Stockbridge dampers," *International journal of non-linear Mechanics,* vol. 37, pp. 1453-1459, 2002.

[15] O. Barry, J. W. Zu, and D. C. D. Oguamanam, "Nonlinear dynamics of Stockbridge dampers," *Journal of Dynamic Systems, Measurement, and Control,* vol. 137, p. 061017, 2015.

[16] N. K. Vaja, O. Barry, and B. DeJong, "Finite Element Modeling of Stockbridge Damper and Vibration Analysis: Equivalent Cable Stiffness," in *ASME 2017 International Design Engineering Technical Conferences and Computers and Information in Engineering Conference*, 2017.

[17] N. Vaja, O. Barry, and E. Tanbour, "On the modeling and analysis of a vibration absorber for overhead powerlines with multiple resonant frequencies," *Engineering Structures,* vol. 175, pp. 711-720, 2018.

[18] Q. Yin, J. Zhao, Y. Liu, and Y. Zhang, "The approximate calculation of the natural frequencies of a Stockbridge type vibration damper and analysis of natural frequencies' sensitivity to the structural parameters," *Mechanical Sciences,* vol. 12, pp. 863-873, 2021.

[19] Z. M. Zondi and M. A. Kaunda, "Modeling of a mass absorber to suppress wind-induced vibrations of transmission line conductors," in *2021 IEEE 12th International Conference on Mechanical and Intelligent Manufacturing Technologies (ICMIMT)*, 2021, pp. 225-229.

[20] Z. Zondi, M. Kaunda, and T. Ngonda, "Characteristics of the asymmetric Stockbridge damper," in *MATEC Web of Conferences*, 2021, p. 00005.

[21] J. Hannah and R. C. Stephens, "Mechanics of machines: elementary theory and examples," *(No Title),* 1984.

[22] M. Markiewicz, "Optimum dynamic characteristics of stockbridge dampers for dead-end spans," *Journal of sound and vibration,* vol. 188, pp. 243-256, 1995.

[23] G. Diana, A. Manenti, C. Pirotta, and A. Zuin, "Stockbridge-type damper effectiveness evaluation. II. The influence of the impedance matrix terms on the energy dissipated," *IEEE Transactions on Power Delivery,* vol. 18, pp. 1470-1477, 2003.